Topographically-Induced Baroclinic Eddies near a Coastline, with Application to the Northeast Pacific[1]

GORDON E. SWATERS AND LAWRENCE A. MYSAK

Departments of Mathematics and Oceanography, University of British Columbia, Vancouver, B.C., Canada, V6T 1W5

(Manuscript received 12 June 1984, in final form 18 May 1985)

ABSTRACT

A mathematical model is developed to describe the interaction between variable bottom topography and a steady, horizontally-sheared baroclinic coastal current. The topography modeled in this study consists of an offshore seamount and a seaward protrusion of the continental slope. The fluid motions are assumed to conserve potential vorticity on the f-plane, and expressions for the pressure, density, velocity and mass transport fields are obtained using a normal mode analysis and the appropriate Green's function for the horizontal problem.

The theory is applied to the northeast Pacific Ocean in an attempt to model the anticyclonic eddy which has been observed by Tabata west of Sitka, Alaska. The numerical calculations of the model and the observed location, dimensions, velocities and transports of the Sitka eddy are in good agreement.

The axial velocities and dimensions of the calculated eddy field are largest for upstream surface and bottom currents of approximately 5–7 and 1–2 cm s^{-1}, respectively. When the surface current is greater than about 20 cm s^{-1} or less than 0.5 cm s^{-1} there are no closed streamlines on the surface. It is therefore conceivable that the season in which the eddy is usually generated (spring–summer) and the particular years in which the eddy is observed to occur are a consequence of seasonal and interannual changes in the upstream current. In particular, it is conjectured that these interannual current changes (and hence the years of eddy occurrence) may be related to interannual variations in the atmospheric circulation in the Gulf of Alaska, which in turn are sometimes linked with El Niño–Southern Oscillation episodes in the tropical Pacific.

1. Introduction

From an examination of historical oceanographic data collected during 1954–67 in the Gulf of Alaska, Tabata (1967, 1982) noted the occurrence, in a number of years, of a baroclinic, anticyclonic (clockwise-rotating) eddy a few hundred kilometers to the west of Sitka, Alaska (located at 57°N, 135°W). The eddy, hereafter called the "Sitka" or "Tabata" eddy, is typically 200–300 km in diameter, extends to a depth of about 1000 m, and has a maximum surface (axial) speed of the order 40 cm s^{-1} (relative to 1000 db surface).

In any year of occurrence, the eddy generally first appears during the spring–summer period and then persists for about half a year, often slowly moving westward during this period. Since the eddy is not observed every year, interannual effects could be important for its generation. Indeed, Willmott and Mysak (1980) suggested that one possible generation mechanism for the Tabata and other northeast Pacific eddies is atmospherically-forced *interannual* baroclinic planetary waves that undergo multiple reflections at the coastlines of British Columbia and Alaska. However, it has been recognized (Willmott and Mysak, 1980; Tabata, 1982), that topographic irregularities near Sitka could also contribute to the production of the Tabata eddy. The purpose of this paper is to describe a theory of eddy generation by the interaction of a steady coastal current (representative of the northward mean flow along the British Columbia coast) with variable bottom topography.

The topographic features modeled in this paper include the set of seamounts around Pratt seamount (56°N, 143°W) and the seaward protrusion of the base of the continental slope off Baranof Island (see Fig. 1). We show that a northward-flowing, baroclinic, laterally-sheared current on a f-plane encountering this topographic configuration generates a large anticyclonic baroclinic eddy possessing many of the characteristics of the Tabata eddy observed during the spring–summer period.

But what determines the year in which an eddy is formed? As will be seen later, the incident surface flow in our model must be fairly moderate (5 to 20 cm s^{-1}) in order for the eddy to be formed west of Sitka. Such moderate current speeds are likely to occur, for example, after a strong El Niño–Southern Oscillation (ENSO) episode in the tropical Pacific. During the course of such an episode a large negative atmospheric pressure anomaly often develops during winter in the Gulf of Alaska[2] because of teleconnections with the

[1] Dedicated to Susumu Tabata on the occasion of his 60th birthday.

[2] This process is also referred to as the expansion and intensification of the Aleutian low.

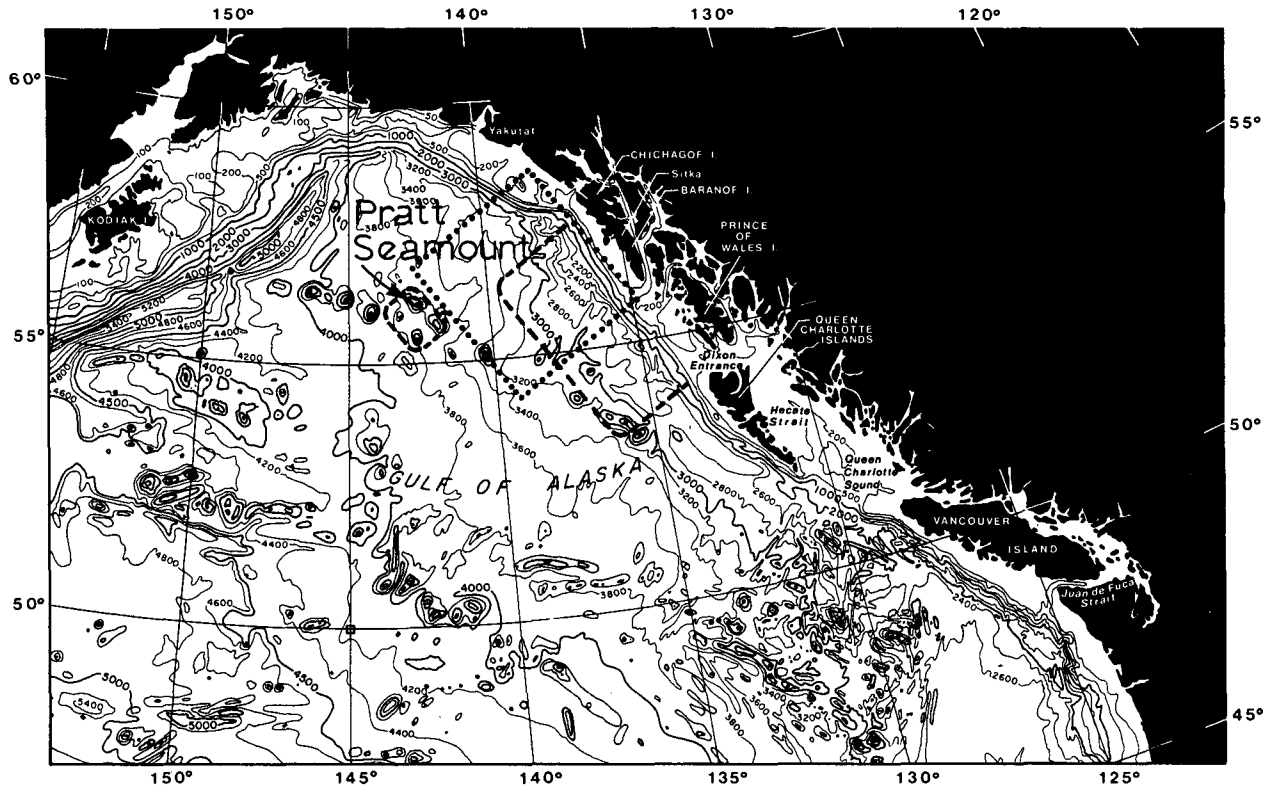

FIG. 1. Bathymetric chart of the northeast Pacific Ocean. The general area of the Sitka eddy is indicated by a dotted square. The base of the topographic features modeled in this paper are marked by dashed lines. The channel model to be introduced later has a width of twice the distance from the coast to Pratt seamount.

equatorial Pacific region (Bjerknes, 1966; Simpson, 1983; Emery and Hamilton, 1985). Such an atmospheric anomaly would help to produce unusually strong northward currents along the British Columbia–Alaska coast and would thus preclude topographic eddy production. However, in the following spring–summer period, the strong cyclonic atmospheric circulation has generally weakened; consequently the coastal currents would tend to be slower and a topographically-induced eddy may arise.[3] In the summer the atmospheric circulation continues to weaken and topographic forcing becomes negligible because of weak upstream currents. At this stage, we spectulate that the β-effect (neglected in our model) becomes important. Hence it may be possible during the late summer and fall to model the Sitka eddy by the superposition of atmospherically-forced, baroclinic planetary waves (Willmott and Mysak, 1980) whose period corresponds to that of the Southern Oscillation, i.e., 3–6 years (Trenberth, 1976; Julian and Chervin, 1978; Horel and Wallace, 1981). At this period high-latitude baroclinic planetary waves (and hence the eddies) travel westward with a speed of about 1 km day^{-1}, which is consistent with the westward eddy speed observed (Tabata, 1982). Also, during this time the eddy could decay due to friction and/or entrainment (e.g., Csanady, 1979; Mied and Lindemann, 1979).

In Section 2 some of the salient features of the Tabata eddy are described, and in Section 3 the mean flow–topographic interaction model is developed. Solutions to the vertical and horizontal boundary value problems are given in Section 4. The theory is applied to the Sitka eddy in Section 5, and the results of a parameter sensitivity analysis are described in Section 6. The results are summarized in Section 7.

2. The anticyclonic baroclinic eddy off Sitka, Alaska

The general area where the Sitka eddy has been observed is indicated by the dotted square in Fig. 1. Data that Tabata (1982) found suitable for examining the eddy came from Gulf of Alaska cruises carried out during the period 1954–67.

Figure 2a hints at the occurrence of an anticyclonic eddy off Sitka (see the eddy 'tip' at 56°N, 137°W) and represents the first partial evidence that Tabata (1982) found for the Sitka eddy. Interestingly enough, Fig. 2a

[3] This senario could also hold for years in which no strong ENSO episode occurs. Emery and Hamilton (1985) have noted that the strong intensification of the Aleutian low during winter sometimes occurs in non-ENSO years (e.g., 1977).

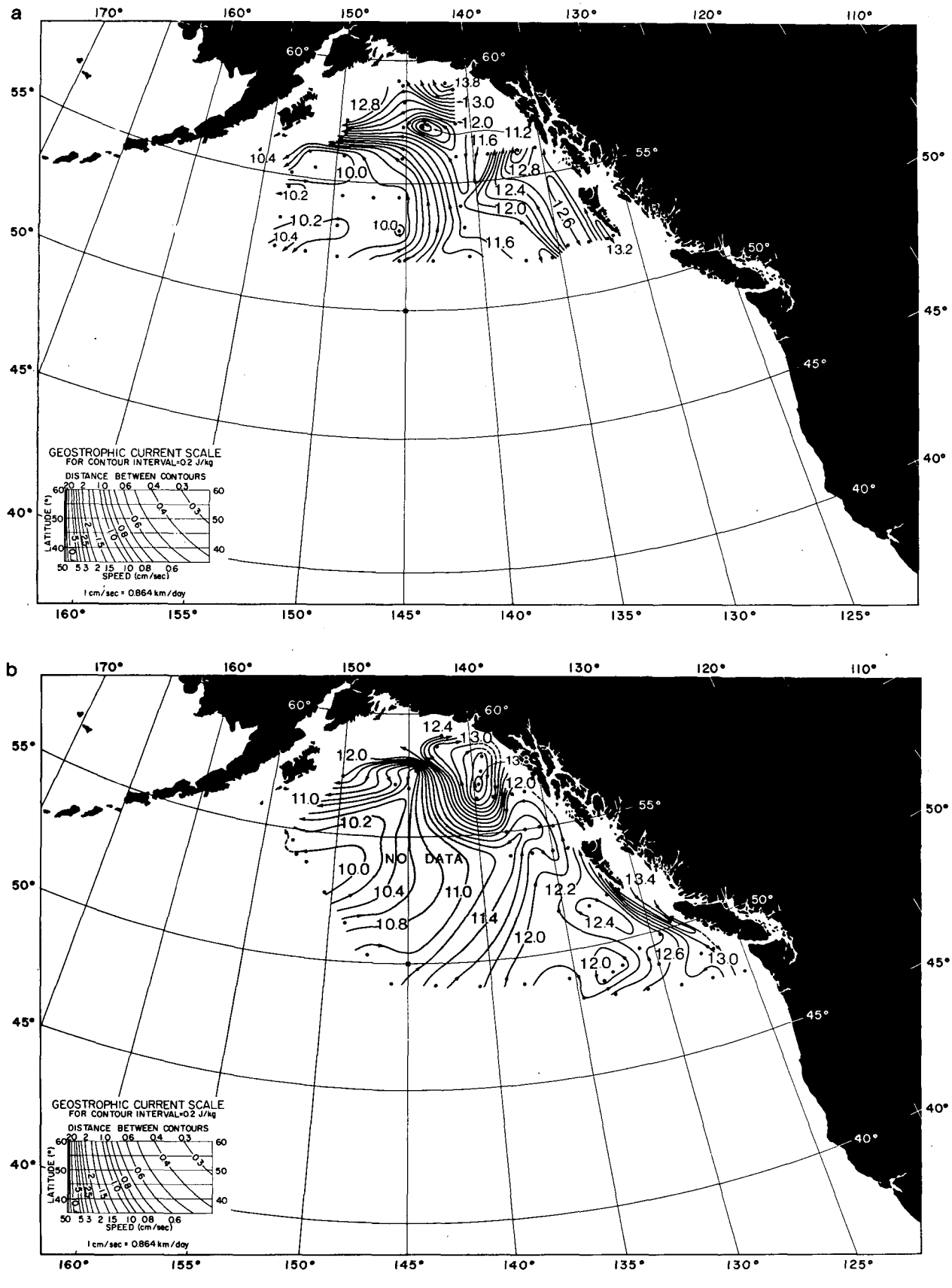

FIG. 2. Geopotential anomaly at the sea surface relative to the 1000 db surface (J kg^{-1}) in the northeast Pacific Ocean: (a) Aug–Sep 1954, (b) Mar–Apr 1958, (c) Jan–Feb 1959, (d) May–Jun 1961. (From Tabata, 1982).

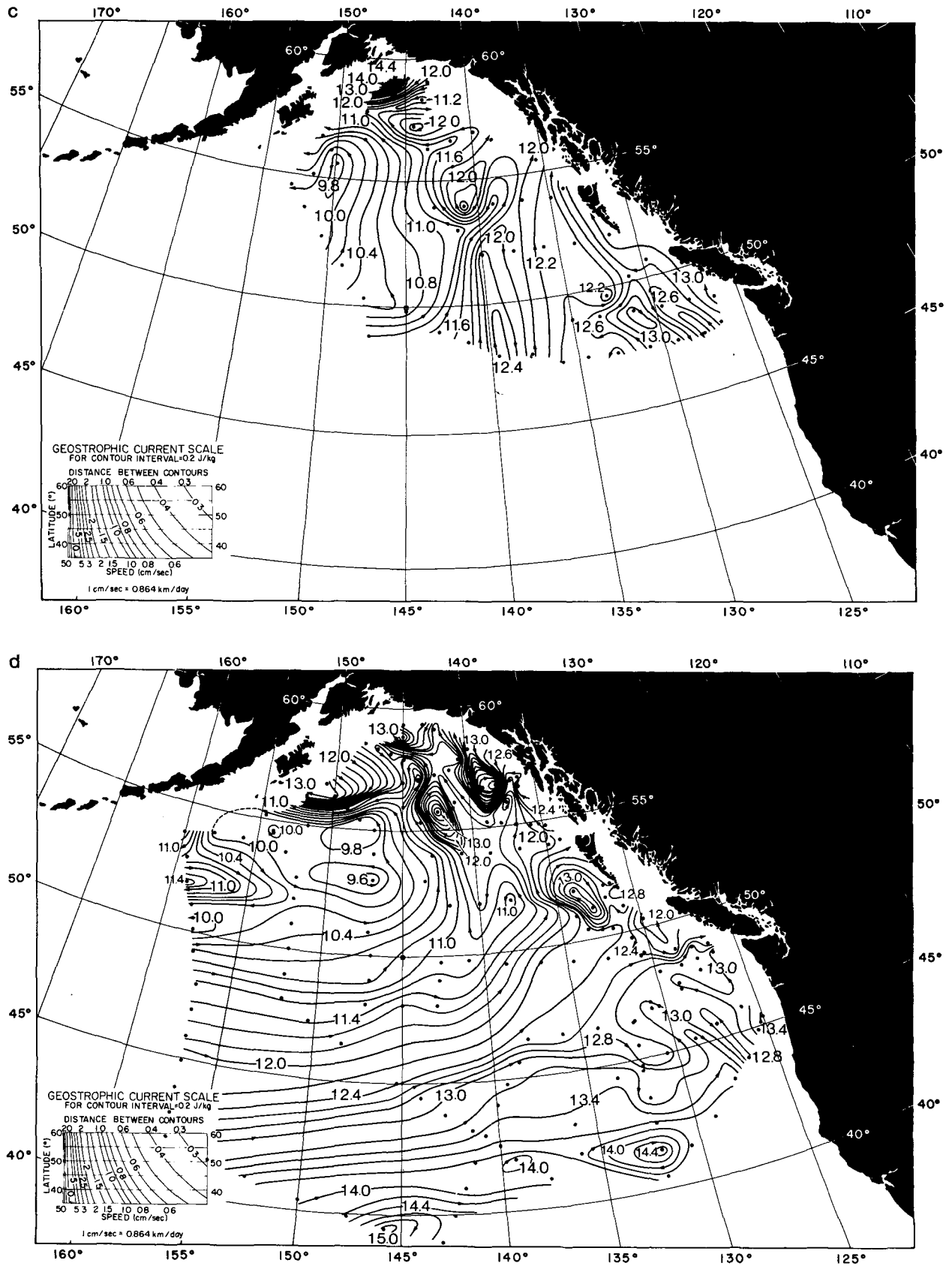

FIG. 2. (*Continued*)

does show the presence of a small cyclonic eddy centered at 57°N, 143°W which, because of its location, could be topographically induced by the flow past the set of seamounts around Pratt seamount (see Fig. 1).

The first clear surface signature of the whole Sitka eddy, however, was found in the spring of 1958 (Fig. 2b). This eddy had a diameter of approximately 300–400 km and was centered at about 57°N, 139°W. It was still located in this region during August 1958 (see Tabata, 1982, his Fig. 2e.), but by next winter the eddy had traveled about 400 km to the southwest (see Fig. 2c). It is interesting to note that this eddy was formed shortly after the 1957–58 ENSO episode.

An anticyclonic eddy similar in size and location to that shown in Fig. 2b was also detected in July–September 1960 (Tabata, 1982). During May–June 1961 on the other hand, two smaller but more intense anticyclonic eddies were found, one off Sitka and the other about 400 km to the southwest (see Fig. 2d).

At the surface, the center of the Tabata eddy is characterized by water of lower salinity rather than by water of a different temperature from that of the neighboring waters. At depth, however, a warm core is often found, generally within the halocline which occurs at depths of 100–200 m and which is depressed at the eddy center. The depression of the isopycnals at the eddy center is evident at the halocline, as well as at depth (see Fig. 7, Tabata, 1982). In some cases where the data was available (e.g., March 1958), this depression could be seen down to 2000 m. Thus we conclude that the eddy penetrates downward to a depth of at least 1000 m, and maybe even to 2000 m. The mean depth of the ocean in this region is about 3500 m.

The ambient geostrophic surface circulation along the British Columbia–Alaska coast consists of a broad northward flow of about 5 cm s^{-1} relative to 1000 db (see Fig. 3). This current is part of the Alaska Stream, which transports water northward at a rate of about $6 \cdot 10^6$ m^3 s^{-1} (Tabata, 1975). Typical transports of the Sitka eddy are comparable to this (see Fig. 9, Tabata, 1982), but the (geostrophic) surface axial speeds (relative to 1000 db) 50 to 100 km radially outward from the eddy center are generally much larger than 5 cm s^{-1}. For the weaker eddies (as in Fig. 2b) the maximum axial speeds (relative to 1000 db) are about 10–20 cm s^{-1} (Table 4, Tabata, 1982). For the intense Sitka eddy observed during May–June 1961, however, the surface speeds relative to 1000 db were as large as 30–40 cm s^{-1} (see Fig. 10, Tabata, 1982).

It may well be that these geostrophic values are an underestimate of the true speeds. For example, near-surface speeds of satellite-tracked buoys (Kirwan *et al.*, 1978) that ended up in the Sitka eddy (see Fig. 11, Tabata, 1982) had values in the range 50–100 cm s^{-1} (Tabata, 1982).

The vertical structure of the northward flowing coastal current varies in the offshore direction (see Fig. 3). Bennett (1959) classified the summer velocity profiles into four categories. Figure 3b shows that the near-coastal current (group IV) is strongly attenuated with depth, with a maximum near-surface speed just under 10 cm s^{-1}. Group II currents, situated immediately west of the group IV currents also monotonically decay with depth although the attenuation is not as severe as with the group IV currents. Typically, group II currents have near-surface maximum speeds on the order of 5 cm s^{-1}. Group III currents, located westward of the British Columbia group II currents have smaller speeds than either group IV or group III currents. Typically they have maximum speeds on the order of 3 cm s^{-1}.

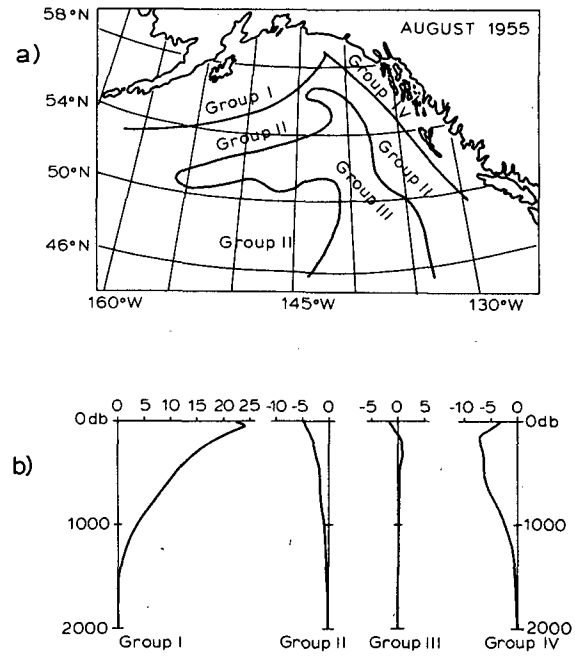

FIG. 3. (a) Approximate regional occurrence of velocity profile types, (b) Geostrophic current of each type relative to 2000 db (cm s^{-1}, negative values indicate northward flow). (From Bennett, 1959).

Thus, in summary, the magnitude of the British Columbia–Alaska coastal current is seen to decay with distance from the coast. A rough estimate of this decay gives an *e*-folding scale of about 80 to 100 km. The current speeds also monotonically decay with depth. However, the vertical shear is fairly weak and is unlikely to provide sufficient potential energy for baroclinic instability, which does occur on the other hand off Vancouver Island (Ikeda *et al.*, 1984).

Figure 3 suggests (see also Fig. 10, Tabata, 1982) that the principal contribution to the transport occurs in the upper ocean. Tabata (1982) calculates that about 75 percent of the transport occurs in the top 500 meters of ocean.

3. Formulation of model

We shall assume that the fluid motions are steady and conserve potential vorticity on the *f*-plane. In non-

dimensional variables this conservation law takes the form [LeBlond and Mysak, 1978, Eq. (44.40)]

$$J[p^{(0)}, \nabla^2 p^{(0)} + \partial_3([S(z)]^{-1}\partial_3 p^{(0)})] = 0 \quad (3.1)$$

where $p^{(0)}$ is the geostrophic pressure field [i.e., the first term in an expansion of the reduced pressure field in the Rossby number ϵ; see (3.5)], ∂_3 denotes the partial derivative in the z (upward) direction, ∇^2 is the horizontal Laplacian and $J[A, B]$ is the Jacobian of A and B. In (3.1), $S(z)$ is given by

$$S(z) = [s_0]^2 \exp[\gamma(z-1)] \quad (3.2)$$

where $s_0 = (N_0 H f^{-1})/L$ = (internal Rossby radius)/(horizontal length scale). The exponential form in (3.2) represents a least squares fit (Willmott and Mysak, 1980) of the Brunt-Väisälä frequency typically observed in the northeast Pacific (Emery *et al.*, 1984). Suitable values of the mean Brunt-Väisälä frequency N_0 and depth H are

$$N_0 = 0.011045 \text{ s}^{-1} \quad H = 3500 \text{ m}, \quad (3.3)$$

whereas the nondimensional scale height $\gamma = \gamma^* H = (254.51 \text{ m})^{-1} \cdot 3500 \text{ m} = 13.75$ (γ^* is the dimensional scale height of the Brunt-Väisälä frequency determined in Willmott and Mysak, 1980). Other parameter values used in this study are

$$L = 400 \text{ km (distance from coast to Pratt seamount)}$$

$$f = 1.2 \times 10^{-4} \text{ s}^{-1} \text{ (at 55°N)}$$

$$U = 1.0 \text{ m s}^{-1} \text{ (horizontal velocity scale)}, \quad (3.4)$$

which imply a Rossby number of

$$\epsilon = U(fL)^{-1} = 0.02. \quad (3.5)$$

It was found that the observed northward-flowing coastal current could be modeled as a zero potential vorticity flow. Therefore the integral of (3.1) is simply

$$[\nabla^2 + \partial_3(S^{-1}\partial_3)]p^{(0)} = 0, \quad (3.6)$$

which is solved in a channel domain given by

$$\{(x, y, z): -\infty < x < +\infty, \quad 0 < y < 2, \ h(x, y) < z < 1\}. \quad (3.7)$$

The variable topography $h(x, y)$ is assumed to be confined to a (finite) region around $x = 0$, and the coast is located at $y = 0$ and the outer channel wall at $y = 2$ (corresponding to a dimensional channel width of 800 km). Numerical calculations (Swaters, 1983) show that such a wall, far enough from the eddy generating region, results in no serious influence on the solutions (see also Ikeda *et al.*, 1984).

The upstream northward baroclinic flow is modeled by

$$u_0 = \exp(-\alpha y)Z(z)$$

$$v_0 = 0,$$

where $Z(z)$ represents the vertical structure of the upstream current. As $|x| \to \infty$ (far from the topography), the lowest order horizontal velocity components are assumed to satisfy $u^{(0)} \to u_0$ and $v^{(0)} \to 0$, or, because of geostrophy

$$p^{(0)} \to \alpha^{-1}(\exp[-\alpha y] - 1)Z(z) \quad \text{as} \quad |x| \to \infty. \quad (3.8)$$

The upstream flow condition corresponds to a horizontally and vertically sheared current. The horizontal shear is exponential with an e-folding length of α^{-1} ($\alpha^{-1}L$ m). The estimated e-folding distance of 80 km for the alongshore current in the northeast Pacific (Fig. 3) implies $\alpha = 5$.

Because the horizontal structure of the upstream current is assumed to decay exponentially away from the coastline, the vertical shear $Z(z)$ must be chosen so that (3.8) satisfies (3.6). Taking $-\partial_2$ (3.6) [i.e., the negative partial y-derivative of (3.6)] and substituting in u_0 implies

$$D_3(S^{-1}D_3 Z) + \alpha^2 Z = 0,$$

where $D_3 = d/dz$.

The normal velocities vanish on the channel boundaries, so that on $y = 0$, $y = 2$ and $z = 1$

$$\partial_1 p^{(0)} = 0 \quad \text{on} \quad y = 0 \quad \text{and} \quad y = 2 \quad (3.9a)$$

$$J[p^{(0)}, S^{-1}\partial_3 p^{(0)}] = 0 \quad \text{on} \quad z = 1. \quad (3.9b)$$

Equation (3.9b) states that $S^{-1}\partial_3 p^{(0)}/p^{(0)}$ is constant along streamlines on $z = 1$. Hence for those streamlines extending upstream (3.9b) implies (Hogg, 1980; Chao *et al.*, 1980)

$$Z\partial_3 p^{(0)} - p^{(0)} D_3 Z = 0 \quad \text{on} \quad z = 1. \quad (3.10)$$

Because the upstream vertical current structure function $Z(z)$ obviously satisfies this boundary condition, the boundary value of $Z(1) = a$ is a free parameter, which is chosen from observations.

Defining $h^*(x^*, y^*) = \epsilon H h(x, y)$, the nondimensional no normal flow bottom boundary condition is

$$w = (u, v) \cdot \nabla h(x, y) \quad \text{on} \quad z = \epsilon h(x, y). \quad (3.11a)$$

Analogously to the derivation of (3.10) the zeroth expansion about $z = 0$ of (3.11a) is

$$Z\partial_3 p^{(0)} - p^{(0)} D_3 Z = -ZSh(x, y) \text{ on } z = 0. \quad (3.11b)$$

Since $h(x, y)$ is assumed to have compact support, $h(x, y) = 0$ as $|x| \to \infty$, which implies that $Z(z)$ satisfies this boundary condition. Therefore $Z(0) = b$ is also a free parameter obtained from observations. Based on the data presented in Section 2 we take $a = 0.1$ and $b = 0.01$, corresponding to an alongshore upstream current with surface and bottom speeds 10 and 1 cm s^{-1}, respectively.

The boundary conditions (3.10) and (3.11b) will be applied to the entire flow field. Although these two boundary conditions have made explicit use of streamlines extending to infinity, which is not the case in the

interior of an eddy, an *ansatz* such as this is required since no general method is known for integrating (3.9b) and the zero-order (3.11a) in an eddy interior (Hogg, 1980). The adoption of (3.10) and (3.11b) as the uniform surface and bottom boundary conditions will ensure continuity of the vorticity field along the eddy boundary.

The idealized topography we take in this paper has the form

$$h(x, y) = h_1 \cos(\pi x) \cos(\pi y)$$

for

$$|x| < 0.5, \quad 0 < y < 0.5 \tag{3.12}$$

$$= h_2 \cos[4\pi(x - 0.6)] \cos[4\pi(y - 0.75)]$$

for

$$|x - 0.6| < 0.125 \text{ and } |y - 0.75| < 0.125 \tag{3.13}$$

$$= 0 \quad \text{for all other } x \text{ and } y,$$

where h_1 and h_2 are defined as $h_i = h_i^*/(\epsilon H)$ with h_i^* the maximum dimensional height of topographic feature i. Figure 4 shows a three-dimensional map of the idealized topography, with heights exaggerated 25 times with respect to lengths. The support of $h(x, y)$ was obtained by examining Fig. 1 and estimating the relevant horizontal length scales.

The form of $h(x, y)$ given by (3.12) corresponds to the continental slope protrusion extending seaward a distance of 200 km. The form of $h(x, y)$ given by (3.13) models the collection of seamounts in the immediate vicinity of the Pratt seamount as a smooth orographic feature with the nondimensional height corresponding to that of the Pratt seamount. The dimensional horizontal scale of this feature is 100 km.

The solution of (3.6) through (3.11) is written in the form

$$p^{(0)} = \alpha^{-1}[\exp(-\alpha y) - 1]Z(z) + p(x, y, z), \tag{3.14}$$

where p corresponds to the topographically induced pressure field. Substituting into (3.6)–(3.11) implies that $p(x, y, z)$ must satisfy

$$[\nabla^2 + \partial_3(S^{-1}\partial_3)]p = 0 \tag{3.15}$$

subject to the boundary conditions,

$$p \to 0 \quad \text{as} \quad |x| \to \infty \tag{3.16}$$

$$p = 0 \quad \text{on} \quad y = 0 \quad \text{and} \quad y = 2 \tag{3.17}$$

$$Z\partial_3 p - pD_3 Z = 0 \quad \text{on} \quad z = 1 \tag{3.18}$$

$$Z\partial_3 p - pD_3 Z = -ZSh \quad \text{on} \quad z = 0. \tag{3.19}$$

The function $Z(z)$ satisfies

$$D_3(S^{-1}D_3 Z) + \alpha^2 Z = 0, \tag{3.20}$$

subject to the boundary conditions

$$Z(0) = b, \quad Z(1) = a. \tag{3.21}$$

The boundary condition (3.17) follows from (3.9a) and (3.16). The physical implication is that no net down channel transport can be created from topographic mean flow interaction. No restriction is made on the order of magnitude of $p(x, y, z)$. In fact $p = O\{\alpha^{-1}[\exp(-\alpha y) - 1]Z\}$ if flow reversal is to occur.

The function $p(x, y, z)$ is found via the following normal mode decomposition (Chao *et al.*, 1980):

$$p = \sum_{n=0}^{\infty} P_n(x, y)G_n(z), \tag{3.22}$$

where $G_n(z)$ is the nth orthonormal eigenfunction solution of

$$D_3(S^{-1}D_3 G_n) + \lambda_n G_n = 0 \tag{3.23}$$

subject to the boundary conditions

$$ZD_3 G_n - G_n D_3 Z = 0 \quad \text{on} \quad z = 0 \quad \text{and} \quad z = 1 \tag{3.24}$$

$$\int_0^1 G_n(z)G_m(z)dz = \delta_{nm}, \tag{3.25}$$

where δ_{nm} is the Kronecker delta function.

The governing equations for the cross-stream functions $P_n(x, y)$ are obtained by multiplying (3.23) by $p(x, y, z)$ and vertically integrating, yielding for each mode

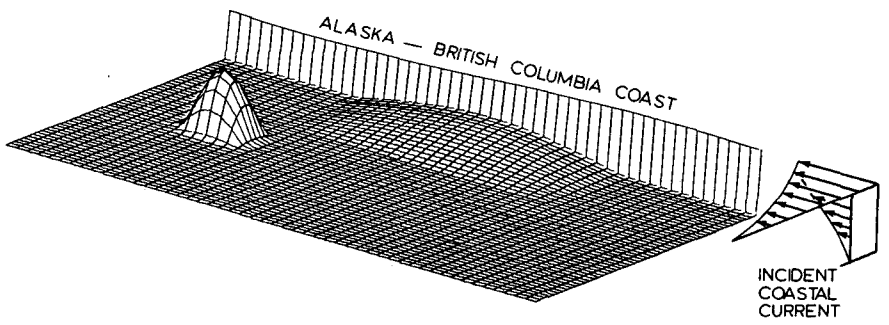

FIG. 4. Three-dimensional contour plot of model topography [$h(x, y)$ given by (3.12) and (3.13)]. Heights are exaggerated 25 times with respect to lengths. Schematic sketch of incident coastal current is shown in lower right corner.

$$(\nabla^2 - \lambda_n)P_n = -G_n(0)h(x, y) \qquad (3.26)$$

subject to the boundary conditions

$$P_n = 0 \quad \text{on} \quad y = 0 \quad \text{and} \quad y = 2 \qquad (3.27)$$

$$P_n \to 0 \quad \text{as} \quad |x| \to \infty. \qquad (3.28)$$

4. Solution of the interaction streamfunction

a. Upstream vertical current structure

The solution of (3.20) subject to (3.21) is (Bryan and Ripa, 1978)

$$Z(z) = \exp(\gamma z/2)\{C_1 J_1[\mu \exp(\gamma z/2)] + C_2 Y_1[\mu \exp(\gamma z/2)]\}, \qquad (4.1)$$

with

$$\mu = (2\alpha/\gamma)[s_0 \exp(-\gamma)]^{1/2} \qquad (4.2)$$

$$C_1 = C_0\{bY_1[\mu \exp(\gamma/2)] - aY_1[\mu] \exp(-\gamma/2)\} \qquad (4.3)$$

$$C_2 = C_0\{aJ_1[\mu] \exp(-\gamma/2) - bJ_1[\mu \exp(\gamma/2)]\} \qquad (4.4)$$

$$C_0 = \{J_1[\mu]Y_1[\mu \exp(\gamma/2)] - J_1[\mu \exp(\gamma/2)]Y_1[\mu]\}^{-1}. \qquad (4.5)$$

Figure 5 shows a graph of $Z(z)$ versus z when $a = 0.1$ and $b = 0.01$ (with $\alpha = 5$). We note that the modeled upstream current is surface intensified, in agreement with the observations.

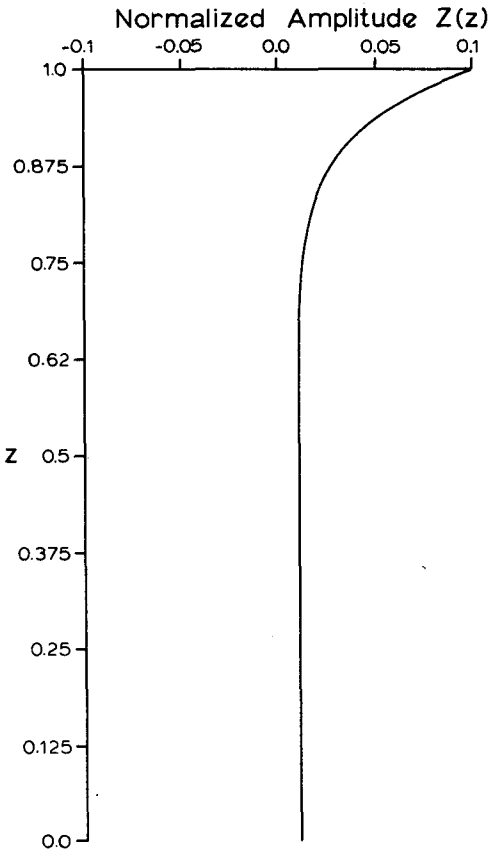

FIG. 5. Vertical structure $Z(z)$ of nondimensionalized upstream current for the case $\alpha^2 = 25$.

b. Vertical mode eigenfunctions and eigenvalues

The solution of (3.23), (3.24) and (3.25) for $G_n(z)$ is

$$G_n(z) = \exp(\gamma z/2)\{A_n J_1[c_n \exp(\gamma z/2)] + B_n Y_1[c_n \exp(\gamma z/2)]\}, \qquad (4.6)$$

where

$$A_n = K_n\{(c_n\gamma/2)Y_0(c_n) - [D_3 Z(0)/Z(0)]Y_1(c_n)\},$$

$$B_n = -K_n\{(c_n\gamma/2)J_0(c_n) - [D_3 Z(0)/Z(0)]J_1(c_n)\},$$

with

$$K_n = \{b_n[(c_n\gamma/2)J_0(c_n) - [D_3 Z(0)/Z(0)]J_1(c_n)]^2 + a_n[(c_n\gamma/2)Y_0(c_n) - [D_3 Z(0)/Z(0)]Y_1(c_n)]^2\}^{-1/2},$$

in which

$$a_n = \{(c_n)^2\gamma\}^{-1}[\{xJ_0(x)\}^2 - 2J_0(x)J_1(x) + \{xJ_1(x)\}^2]\Big|_{x=c_n}^{x=c_n \exp(\gamma/2)}$$

$$b_n = \{(c_n)^2\gamma\}^{-1}[\{xY_0(x)\}^2 - 2Y_0(x)Y_1(x) + \{xJ_1(x)\}^2]\Big|_{x=c_n}^{x=c_n \exp(\gamma/2)}$$

$$c_n = (2/\gamma)[\lambda_n s_0 \exp(-\gamma)]^{1/2}. \qquad (4.7)$$

The parameters c_n are the discrete denumerable solutions of

$$\{(c_n\gamma/2) \exp(\gamma/2)Y_0[c_n \exp(\gamma/2)] - [D_3 Z(1)/Z(1)]Y_1[c_n \exp(\gamma/2)]\} \times \{(c_n\gamma/2)J_0(c_n) - [D_3 Z(0)/Z(0)]J_1(c_n)\}$$

$$= \{(c_n\gamma/2) \exp(\gamma/2)J_0[c_n \exp(\gamma/2)] - [D_3 Z(1)/Z(1)]J_1[c_n \exp(\gamma/2)]\} \times \{(c_n\gamma/2)Y_0(c_n) - [D_3 Z(0)/Z(0)]Y_1(c_n)\} \qquad (4.8)$$

with the eigenvalue λ_n related to c_n by inverting (4.7) to obtain $\lambda_n = [\gamma c_n/2]^2(s_0)^{-1} \exp(\gamma)$.

Figure 6 shows $G_0(z)$, $G_1(z)$ and $G_2(z)$ when $Z(0) = 0.01$, $Z(1) = 0.1$ and $\alpha = 5$. The exponential decay with depth occurs for each mode because $S(z)$ decays exponentially with depth [see (3.2)]. Swaters (1983) has shown that $\lambda_0 = \alpha^2$ and that $G_0(z) = Z(z)/\{\int_0^1 Z^2(z)dz\}^{1/2}$; thus $G_0(z)$ is surface intensified because $Z(z)$ is also.

c. Solution of the horizontal problem

The solution for the cross-stream function P_n is obtained in the form

$$P_n(x, y) = \int_{-\infty}^{\infty} \int_0^2 g(x, y|x_0, y_0)h(x_0, y_0)dy_0dx_0 \tag{4.10}$$

where $g(x, y|x_0, y_0)$ is the Green's function for (3.26) and (3.27) given by (Swaters, 1983)

$$g = \sum_{m=1}^{\infty} \{G_n(0)[b_{nm}]^{-1/2} \sin(m\pi y/2) \times \sin(m\pi y_0/2) \exp[-|x - x_0|(b_{nm})^{1/2}]\}. \tag{4.11}$$

Evaluation of the integral (4.10) gives

$$P_n = h_1G_n(0) \sin(\pi y)R_{n2}(x)[2\pi(\pi^2 + \lambda_n)(2\pi^2 + \lambda_n)]^{-1} + \sum_{m=1}^{\infty} h_1G_n(0) \sin(m\pi y/2)R_{nm}(x)[m/2 - \sin(m\pi/4)]$$
$$\times [\pi(m^2/4 - 1)(b_{nm})(b_{nm} + \pi^2)]^{-1} - \sum_{m=1}^{\infty} 4h_2G_n(0) \sin(m\pi y/2)S_{nm}(x)[\sin(7\pi m/16)$$
$$+ \sin(5\pi m/16)][\pi(m^2/4 - 1)(b_{nm})(16\pi^2 + b_{nm})]^{-1},$$

where the functions R_{nm} and S_{nm} are given by

$$R_{nm}(x) = 2\pi \exp[-|x|(b_{nm})^{1/2}] \cosh[(b_{nm})^{1/2}/2], \quad \text{if} \quad |x| > 0.5$$
$$R_{nm}(x) = 2(b_{nm})^{1/2} \cos(\pi x) + 2\pi \exp[-(b_{nm})^{1/2}/2] \cosh[x(b_{nm})^{1/2}], \quad \text{if} \quad |x| < 0.5$$
$$S_{nm}(x) = 8\pi \exp[-|x - 0.6|(b_{nm})^{1/2} \cosh[(b_{nm})^{1/2}/8], \quad \text{if} \quad |x - 0.6| > 0.125$$
$$S_{nm}(x) = 2((m\pi/4)^2 + \lambda_n)^{1/2} \cos[4\pi(x - 0.6)] + 8\pi \exp[-(b_{nm})^{1/2}/8] \cosh[(x - 0.6)(b_{nm})^{1/2}], \quad \text{if} \quad |x - 0.6| < 0.125,$$

with $b_{nm} = (m\pi/2)^2 + \lambda_n$. Calculation of the velocity, density and transport fields is given in the Appendix.

5. Application to the Sitka (Tabata) eddy

The oceanographic and bathymetric data for the northeast Pacific suggest that suitable values for N_0, $(\gamma^*)^{-1}$, a, b, α, h_1 and h_2 are 0.011045 s^{-1}, 254.51 m, 0.1, 0.01, 5.0, 10.9 and 34.1 respectively. This set of parameters yields $\lambda_0 = 25$, $\lambda_1 = 382.86$, $\lambda_2 = 2219.01$, $\lambda_3 = 5584.99$, $\lambda_4 = 10394.55$ and $\lambda_5 = 16642.86$ for the first six eigenvalues. The numerical calculations contained the first twelve vertical modes ($n \leq 11$) and the first twenty cross-channel modes ($m \leq 20$). Addition of higher modes had no noticable effect on the computed quantities to double precision accuracy.

The structure of the solutions are summarized in the form of contour and stick plots in Figs. 7, 8, 9 and 10. The surface streamlines are shown in Fig. 7a (horizontal contour plot of $p^{(0)}[z = 1]$, contour intervals ± 0.01).

The surface streamlines delineate three flow features. Over the seamount [centered at $(x, y) = (0.6, 0.75)$] and over the slope protrusion ($-0.5 < x < 0.5$, $0 < y < 0.5$) are two anticyclonic eddies. Encircling both local features is a large-scale anticyclonic circulation. The outer boundary of this large scale circulation is formed by the zero streamline, which bifurcates on $y = 0$ (the coast) at $x \approx \pm 0.6$.

The radius of the encircling flow is about 0.5 (200 km), which is of similar scale to Tabata's (1982) estimate of the radius of the Sitka eddy (100 to 150 km—see Fig. 2b–d). The center of the computed large-scale

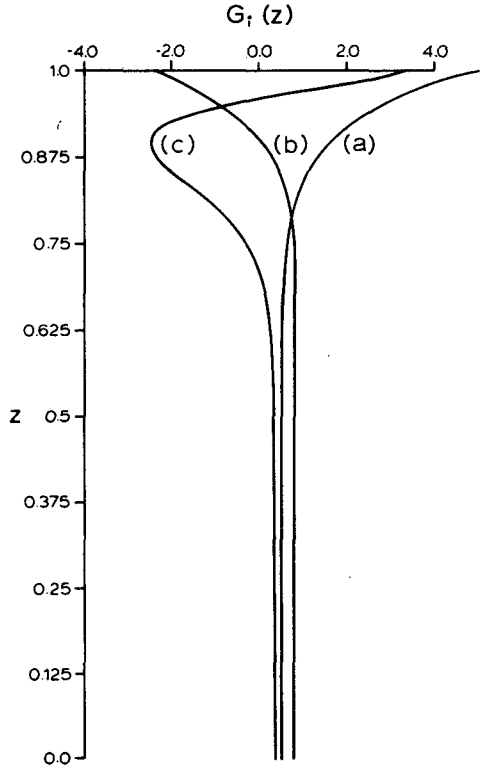

FIG. 6. First three vertical modes, (a) $G_0(z)$, (b) $G_1(z)$, (c) $G_2(z)$.

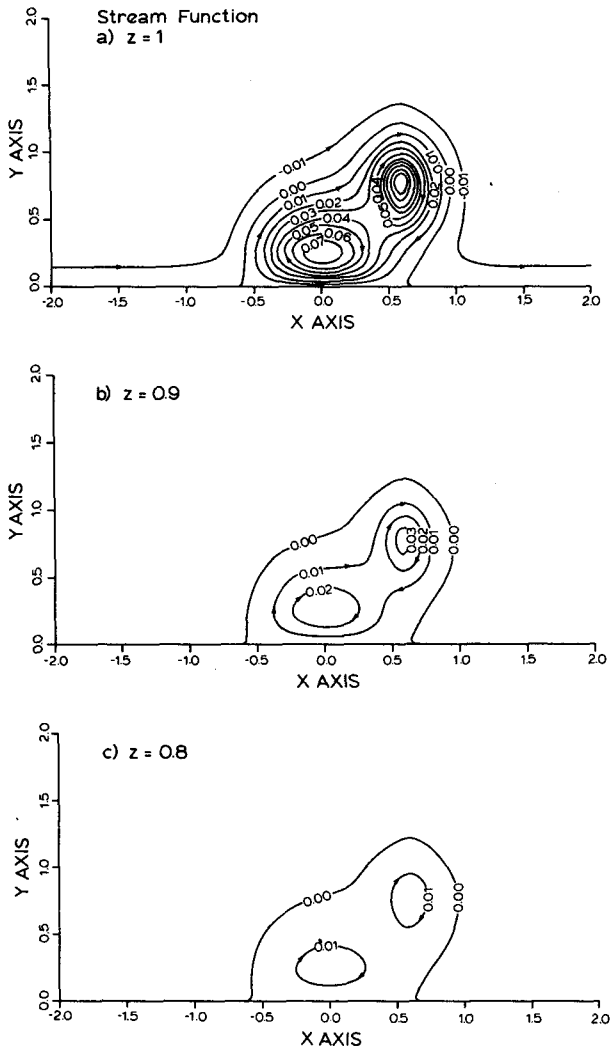

FIG. 7. Horizontal contour plots of $p^{(0)}$ (contour increment is ±0.01), (a) on $z = 1$ (surface), (b) on $z = 0.9$ (350 m deep) and (c) on $z = 0.8$ (700 m deep).

circulation is approximately at $(x, y) = (0.25, 0.5)$ which corresponds approximately to 57°N, 138°W, consistent with Tabata's (1982) location for the center of the Sitka eddy (e.g., see Fig. 2d).

As depth increases our solution describes decreasing flow. This is because the principal structure is determined by the $n = 0$ mode and $G_0(z)$ is surface intensified (see Fig. 6). Figure 7b (contour plot of $p^{(0)}[z = 0.9]$, 350 meters deep, contour intervals ±0.01) illustrates the decay. Extreme values of $p^{(0)}$ on $z = 1$ occur over the seamount ($p^{(0)} \approx 0.1$) and over the slope protrusion ($p^{(0)} \approx 0.08$). At a depth of 350 meters these values have decayed to 0.04 and 0.03, respectively. Figure 7c depicts the streamlines on $z = 0.8$ (700 meters deep, same contour intervals). The flow is further reduced with $p^{(0)} \approx 0.01$ over both the slope protrusion and the seamount.

The surface intensification in the calculated flow field can also be seen in Fig. 8a–c (contour plots of vertical sections of $p^{(0)}$ along $y = 0.2$, 0.4 and 0.6, respectively, contour intervals ±0.01). These figures show that the significant vertical variation in $p^{(0)}$ is constrained to the upper 1100 meters of ocean. Below this depth $p^{(0)}$ is substantially uniform compared to the surface layer and thus the calculated eddy appears surface trapped and intensified.

Observations of the isopycnal depression suggest a vertical extent of the eddy on the order of a kilometer (see Fig. 7, Tabata, 1982), with March 1958 and January 1960 data suggesting that the isopycnals deflections persisted as deep as 2000 meters (Tabata, 1982). Vertical sections of $\rho^{(0)}$ [see (A3)] along $y = 0.2$, 0.4 and 0.6 (Figs. 9a–c, respectively, contour intervals ±0.1) show that the sharpest gradients in $\rho^{(0)}$ occur in

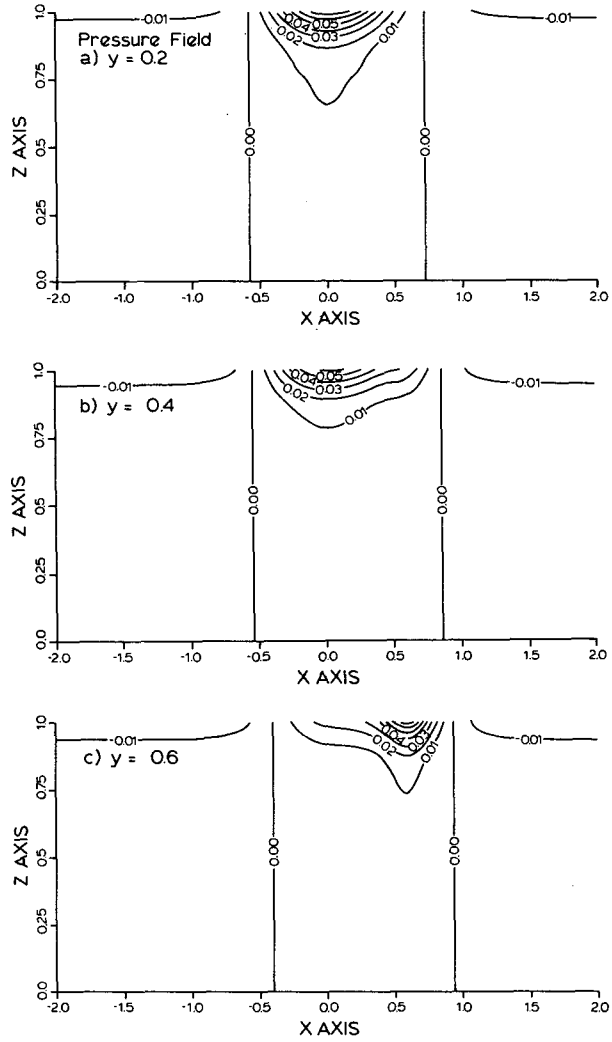

FIG. 8. Contour plots of vertical sections of $p^{(0)}$ (contour increment is ±0.01), (a) on $y = 0.2$ (80 km offshore), (b) on $y = 0.4$ (160 km offshore) and (c) on $y = 0.6$ (240 km offshore).

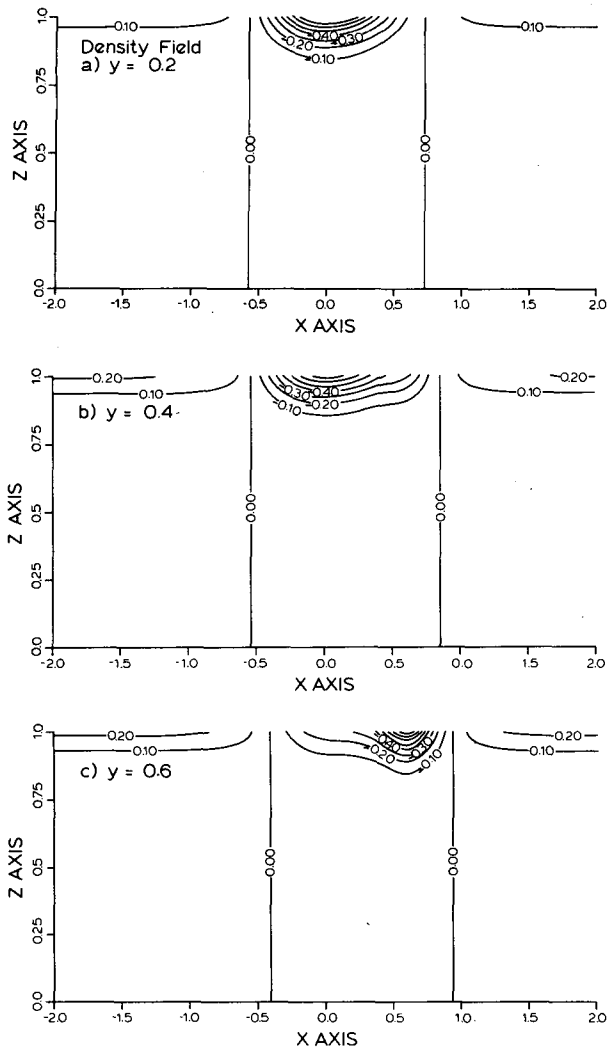

FIG. 9. Contour plots of vertical sections of $\rho^{(0)}$ (contour increment is ±0.1), (a) on $y = 0.2$ (80 km offshore), (b) on $y = 0.4$ (160 km offshore) and (c) on $y = 0.6$ (240 km offshore).

the upper 900 meters of the ocean. Thus estimates of the vertical extent of the calculated eddy based on the pressure and density fields are on the order of 1000 meters, which is in agreement with the observations.

Both the seamount and the slope protrusion are necessary to produce an eddy which has the geographical location and horizontal size of the Sitka eddy. If $h_1 = 0$ (i.e., no slope protrusion) the resulting flow has a single (radius 50 km) anticyclonic eddy over the seamount, and if $h_2 = 0$ (i.e., no seamount) the resulting flow has a single anticyclonic eddy (radius 50 km) over the slope protrusion (Swaters, 1983). These calculations suggest that the topographic configuration of slope protrusion and seamount is necessary in order that the calculated solutions agree with the size and location of the Sitka eddy. Our solution for this topographic configuration suggest a marked turning of the near coastal current toward the Pratt seamount beginning southward of the slope protrusion (see Fig. 7). This seaward deflection of the alongshore currents is observed in the data (S. Tabata, private communication, 1983). Effects of variations in h_1 and h_2 are discussed further in the next section.

Figures 10a, b, and c show stick plots of the horizontal velocity field [obtained from (A1) and (A2)] on $z = 1$, 0.9 and 0.8, respectively. Near-surface speeds for the Sitka eddy were inferred by Tabata (1982) from satellite-tracking buoys (Kirwan *et al.*, 1978; see also Fig. 11, Tabata, 1982) which in 1977 entered the northwest area of the Sitka eddy (Tabata, 1982). We take the northwest sector to be around (x, y) coordinates (0.75, 1.25). The average drift rate for these buoys was computed to be 62, 91 and 47 cm s^{-1}, with the latter average obtained from a drogued buoy. Our solutions for this region predict surface drift axial speeds between 30 and 40 cm s^{-1}. Hence the calculations are consistent with the drogue buoy results but are an underestimate of the value obtained from the undrogued buoys.

Tabata's estimates of the southward buoy drift rate in the northeast sector of the Sitka eddy is between 48 and 64 cm s^{-1}. Assuming the northeast sector to be in the general neighborhood of (x, y) coordinates (0.5, 0.25), our solutions predict southward surface speeds on the order of 50 cm s^{-1} in this region (see Fig. 10a).

Subsurface current speeds in the interior of the water column in the eddy are consistent with the observations of the Sitka eddy. Relative to the 2500 db level, Tabata estimates a 1.5 cm s^{-1} current at the 2000 db level. At the 1750 m depth level the model gives a current of 2 cm s^{-1} over the slope protrusion and 3 cm s^{-1} over the seamount.

Tabata (1982) computed the volume transport along 100 km sections. To compare with these calculations, the expressions for the transports, (A5) and (A6), were averaged over similar 100 km sections. (The northward transports were averaged over y and the eastward transport were averaged over x.) Tabata (1982) reports that the upstream coastal current has a transport on the order of 6 Sv ($\equiv 6 \times 10^6$ cm^3 s^{-1}). Our solution for the upstream current predicts an alongshore transport of 5.9 Sv. As distance from the coast increases, the transport decreases since the current is exponentially sheared.

The transports computed in the eddy were in the main consistent with those observed by Tabata (1982). The large scale anticyclonic circulation (shown in Fig. 7 as exterior to the smaller local eddies) has a transport of about 4 Sv. This compares favorably with Tabata's observation of 5 Sv (see Fig. 9 in Tabata, 1982). The local eddies produced over the slope protrusion and the seamount had maximum computed transports on the order of 15–20 Sv. These estimates are approximately twice as large as the observed values. Over the slope protrusion, Tabata (1982) estimates a southward transport of about 8 Sv (see Fig. 9, Tabata, 1982), and over the Pratt seamount the observed transport is be-

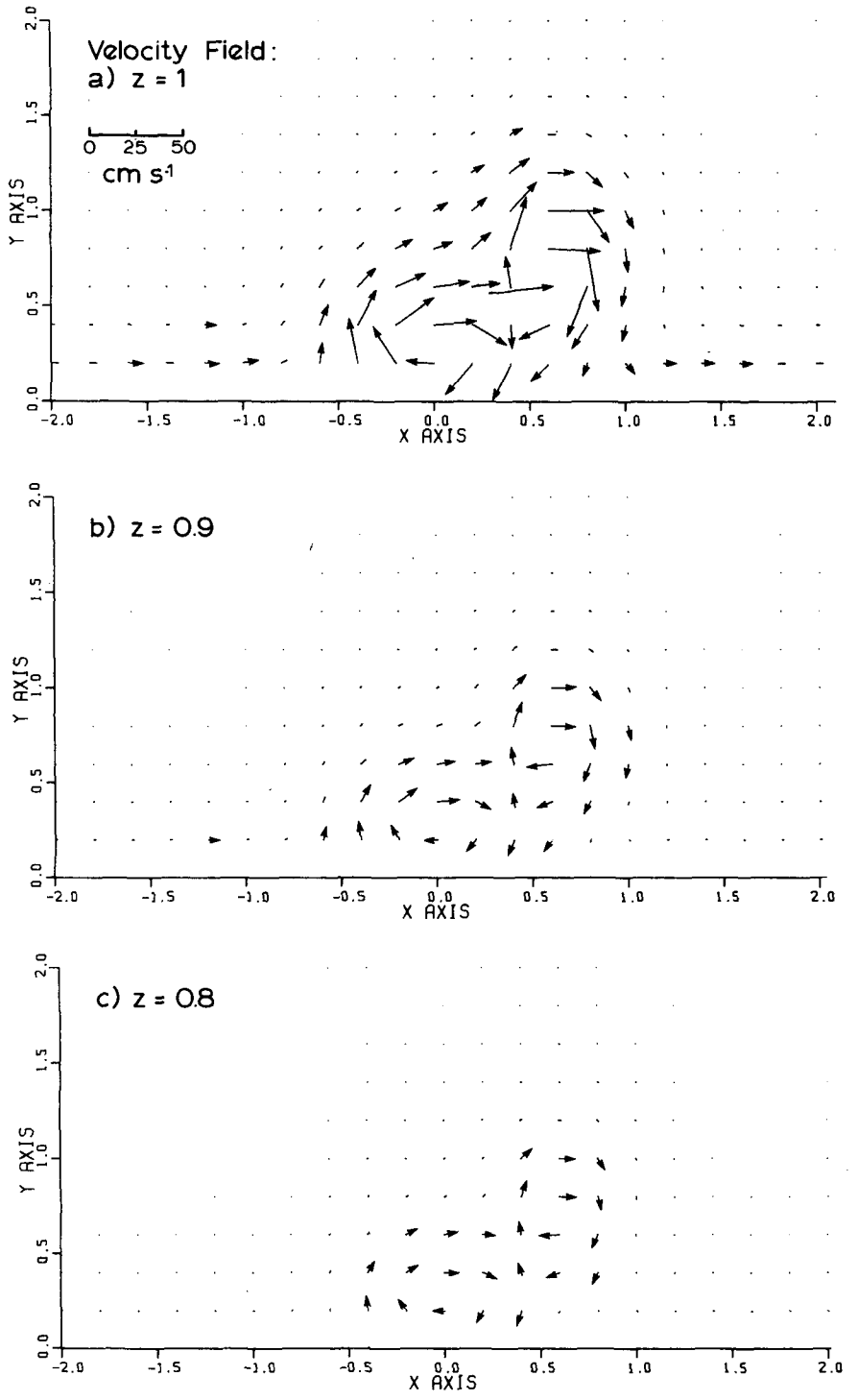

FIG. 10. Eulerian horizontal velocity field ($u^{(0)}$, $v^{(0)}$), (a) on $z = 1$ (surface), (b) on $z = 0.9$ (350 m deep) and (c) on $z = 0.8$ (700 m deep).

tween 5 and 6 Sv. The discrepancy between the observed and theoretical transports directly over the topography is probably due to bottom and side friction, which has been neglected in our model.

6. Parameter sensitivity analysis

An extensive investigation of the effects of parameter variations on the solution was carried out by Swaters

(1983). Here we now summarize some of the results of this parameter study and point out a few interesting implications. The parameters to be discussed are ϵ, h_1, h_2, a, b, and α.

Variations in the Rossby number (within the context $\epsilon \ll 1$) are best understood from the relationship between ϵ and the topographic parameters h_1 and h_2 ($h_i = h_i^*/(\epsilon H)$, see Section 3). Increasing (decreasing) ϵ decreases (increases) the magnitude of h_1 and h_2, which in turn will decrease (increase) the magnitude of the horizontal amplitude functions $P_n(x, y)$.

Huppert (1975) has shown for a single topographic feature that the parameter $H_0(\epsilon H)^{-1}$ (H_0 is Huppert's maximum dimensional topographic height) must be greater than some critical O(1) value (depending on the upstream flow and topographic geometry) in order for a stagnation point to exist in the flow, which is a necessary condition for the existence of a (stratified) Taylor column. When more than one topographic feature is present different critical values may be obtained for the formation of a local eddy over each topographic feature.

Numerical experiments (Swaters, 1983) suggested that $h_1 > 4$ for an eddy to be formed over the slope protrusion, and $h_2 > 9$ for an eddy to be formed over the seamount. Because these critical values for h_1 and h_2 are different, it follows that increasing the Rossby number will result in one or two local eddies forming in the flow as one or the other of h_1 and h_2 nears its critical value. Increasing ϵ to about 0.075 prevents an eddy from forming over the slope protrusion, but allows an eddy to form over the seamount. If $\epsilon > 0.1$ our solutions do not display any closed streamlines and thus no eddy is produced anywhere in the flow. Decreasing ϵ increases the topographic parameters, resulting in an intensification in the interaction between the flow and the topography.

The parameter α determines the upstream horizontal current shear. If α increases, the upstream current becomes more coastally trapped. Decreasing α broadens the coastal flow.

Consider α in the Green's function as written in (4.11), and recall that $\lambda_0 = \alpha^2$. Increasing (decreasing) α will decrease (increase) the magnitude of $g(x, y|x_0, y_0)$ for a given $(x, y|x_0, y_0)$. Consequently, decreasing (increasing) α will intensify (weaken) the interaction between the upstream flow and the coastal topography. For a detailed discussion on the effect of variations of α on the eddy field, see Swaters (1983).

We discuss now the effect of variations in $Z(0)$ and $Z(1)$ on the calculated eddy field. For sufficiently large $Z(0)$ Swaters (1983) has shown that no eddy is produced. The "cutoff" value for the bottom boundary current was numerically determined to be about 50 cm s^{-1}, assuming all other parameters are held to their standard values. At the other extreme $Z(0) = 0$ will also imply no interaction. It is clear that each $P_n(x, y)$ is proportional to $G_n(0)$ (see the expression for $P_n(x, y)$ given in Section 6). From (3.24) it follows that if $Z(0) = 0$ then $G_n(0) = 0$ for each mode (assuming $D_3 Z(0) \neq 0$). Since the intensity of the eddy field weakens for sufficiently large or small upstream bottom currents there must be some value of $Z(0)$ for which the interaction field is maximized. For the standard set of parameters this value is approximately 0.01–0.02 (1–2 cm s^{-1}).

Swaters (1983) has shown that for a sufficiently large surface current [i.e., $Z(1)$] no eddy is produced. If all other parameters are held to their standard (northeast Pacific) values, numerical experiments suggest that this "cutoff" speed is about 30 cm s^{-1}. As $Z(1)$ approaches this "cutoff" speed from below, the surface expression of the eddy weakens. For surface speeds on the order of 20–25 cm s^{-1} a submerged baroclinic anticyclonic is produced in the region $z < 0.75$, but no closed streamlines occur in the near-surface region. Increasing (decreasing) the horizontal current shear parameter α, decreases (increases) the necessary cutoff speed.

In the extreme situation, with $Z(1) = 0$ there is no surface expression of any interaction between the upstream current and the topography. If $Z(1) = 0$ and $D_3 Z(1) \neq 0$, then (3.24) requires $G_n(1) = 0$ and hence $p(x, y, 1) = 0$ [see (3.22)]. The existence of a cutoff surface speed, and the fact that $Z(1) = 0$ leads to $p^{(0)} = 0$ on $z = 1$, implies the existence of a value of $Z(1)$ for which the surface interaction is maximized. For the standard set of parameters this value is about 5–7 cm s^{-1}.

7. Summary and discussion

We have described a quasi-geostrophic theory of baroclinic eddy generation by the interaction of a steady coastal current (representative of the northward mean flow along the British Columbia coast) with bottom topography. Expressions for the pressure, density, velocity and mass transport were obtained for a flow over a continental slope protrusion and an offshore seamount, which exist in the bottom topography off Sitka, Alaska.

The complexity of the observed upstream current did not lend itself to integrating the potential vorticity equation upstream, in the usual manner, to determine the functional relation between the geostrophic pressure $p^{(0)}$ and the potential vorticity $\nabla^2 p^{(0)} + \partial_3(S^{-1}\partial_3 p^{(0)})$. However, it was found that the assumption of a zero potential vorticity flow was able to model the observed northward-flowing coastal current in the northeast Pacific. The horizontal structure of the coastal current was modeled with an exponential and the vertical structure was determined so that the upstream geostrophic pressure was consistent with the zero potential vorticity assumption.

This consistency requirement reduces to solving a two-point boundary value problem for the vertical structure of the upstream current. The horizontal and vertical structure of this current and the computed transports agree with the observations. Also, the results

TABLE 1. Dates of eddy occurrence and corresponding sea level atmospheric circulation in the North Pacific. A strong winter circulation corresponds to an intensification of the climatological Aleutian low, whereas a weak (winter or spring) circulation corresponds roughly to a weakened Aleutian low shifted westward and a weak high pressure intrusion from the southeast.

Date of oceanographic data*	Eddy present near Sitka	Winter (DJF) N. Pacific atmospheric circulation**	Spring (MAM) N. Pacific atmospheric circulation@
Aug–Sep 1954 (Fig. 2a)	Probably (data for region incomplete)	Moderate to strong	Weak
May–Jun 1956	No	Weak	Weak
Jul–Aug 1957	No	Weak	Weak
Mar–Apr 1958† (Fig. 2b)	Yes	Strong	Weak
Jun–Aug	Yes (but eddy observed farther offshore)		
Jan–Feb 1959 (Fig. 2c)	No (but 1958 eddy observed still farther offshore)	Weak to moderate	Weak
Aug–Sep	No		
Jan–Feb 1960	Starting to form	Moderate to strong	Weak
Jul–Sep	Yes		
May–Jun 1961 (Fig. 2d)	Yes	Strong	Weak
May–Jul 1962	No	Weak	Very weak
Feb 1967	No	Weak to moderate	Weak
Mar–May 1977	Yes	Very strong	Weak

* Tabata (1982).
** Emery and Hamilton (1985).
@ Hamilton (1984).
† Second year of strong ENSO episode.

of the numerical calculations of the downstream solution are in good agreement with the observed location, dimensions, velocities and transports of the anticyclonic, baroclinic Sitka eddy.

One interesting property of the calculations is that the upstream surface current must be less than approximately 20 cm s^{-1} for the eddy field to have closed streamlines on the surface. The maximum axial speeds and size of the computed eddy field occur for upstream surface currents of approximately 5–7 cm s^{-1}. When the upstream surface speeds are less than this, the surface eddy circulation is very weak and disappears in limit of no upstream surface current.

It is possible, therefore, that the season (generally spring–summer) and year in which the Sitka eddy is generated may be a consequence of seasonal and interannual variations in the upstream current. The interannual variability in the British Columbia coastal current could be partly due to the expansion and intensification of the Aleutian low, which is often (but not always) associated with a strong El Niño–Southern Oscillation episode. During the winter of such an event (e.g., 1958) the coastal current increases substantially, which probably precludes topographic generation of the Sitka eddy. However, in the following spring–summer period, the Aleutian low weakens; we speculate that this results in slower coastal currents and hence allows the formation of the Sitka eddy (e.g., Fig. 2b). The southwestward movement of the eddy some 6–10 months later (e.g., Fig. 2c) could then be partially explained by the planetary wave mechanism of Willmott and Mysak (1980).

This senario is explored further in Table 1, which tabulates the season and year of eddy occurrence as reported by Tabata (1982), and corresponding strength of the atmospheric circulation during winter (December, January, February) and spring (March, April, May) as determined from sea level pressure maps presented by Emery and Hamilton (1985) and Hamilton (1984). It is remarkable that during each spring–summer in which the eddy has been observed just west of Sitka (in years 1954, 1958, 1960, 1961, 1977), the preceding winter Aleutian low was strong or moderately strong compared to the climatological mean, and the following spring circulation was weak.[4] Conversely, in terms of the oceanographic data available (see also Table 1), when the winter circulation was weak (in years 1956, 1957, 1959, 1962), no eddy was observed in the spring–summer period. The reason for this apparent correlation is not clear, but may be due to an anomalously weak coastal circulation (and hence a weak topographic interaction) throughout each of these years.

The potential effects of the Sitka eddy currents on the lateral distribution of halibut larvae off Baranof Island have already been noted by Tabata (1982). It is also conceivable that the return migration routes and timing of the various Fraser River sockeye salmon stocks could be affected by the presence of the Sitka eddy. It is generally believed (Groot, 1982) that mature Fraser River sockeye salmon begin their return journey from the open ocean to the spawning grounds (in various tributaries of the Fraser River) along the Alaskan Panhandle during spring. If no Sitka eddy is present,

[4] During the 1982–83 ENSO episode, following the winter 1983 intensification of the Aleutian low (Simpson, 1983), a Sitka eddy was observed (March 1983) by means of the UBC IR remote sensing facility (A. Thomas, personal communication, 1984).

the route and timing of the returning salmon might be considered as normal. However, if a strong anticyclonic eddy is present one year during spring (e.g., 1958) and the salmon approach the coast near the southern boundary of this eddy, they would encounter adverse currents and thus take a longer than normal time to make "landfall" on the shelf. Alternatively, the homeward journey could be shortened considerably if during that year the salmon approached the northern side of this eddy during spring. In any event, the interannual occurrence of the Sitka eddy could cause interannual fluctuations in the migration patterns and return times of the salmon, which in turn could produce interannual changes in the fish catch near Vancouver Island (because of the uncertainty as to when and where to find the returning salmon). Mysak *et al.* (1982) have shown that interannual fluctuations in the B.C. sockeye catch are highly coherent with interannual fluctuations in coastal sea surface temperature and sea level. Perhaps this result is also an indirect indication of the influence of changing current conditions in the Sitka eddy region on the B.C. sockeye catch.

Acknowledgments. We are indebted to Dr. S. Tabata for informative discussions about the observations of the Sitka eddy, to Dr. P. H. LeBlond for constructive criticism of the theoretical results, and to Dr. W. A. Perrie for initial theoretical assistance. We also thank Dr. S. Tabata for providing prints of Figs. 1 and 2, and Dr. Kevin Hamilton for comments on a first draft of this paper. This research was supported by the Natural Sciences and Engineering Research Council of Canada through an Operating Grant, and the U.S. Office of Naval Research, Code PO422. G.E.S. also gratefully acknowledges the support of a Teaching Assistantship from the Department of Mathematics, U.B.C., during the tenure of this work.

APPENDIX

Expressions for Velocity, Density and Transport

The O(1) alongshore velocity is given by $u^{(0)} = -\partial_2 p^{(0)}$, i.e.,

$$u^{(0)} = Z(z)\exp(-\alpha y) - \sum_{n=0}^{\infty} \partial_2 P_n G_n, \qquad \text{(A1)}$$

where $\partial_2 P_n$ is given by

$$\partial_2 P_n = h_1 G_n(0)\cos(\pi y) R_{n2}[2(\pi^2+\lambda_n)(2\pi^2+\lambda_n)]^{-1} + \sum_{m=1}^{\infty} h_1 m G_n(0)\cos(m\pi y/2) R_{nm}[m/2 - \sin(m\pi/4)] \times \{2(b_{nm})(m^2/4-1)[(m\pi/2)^2+\pi^2+\lambda_n]\}^{-1} - \sum_{m=1}^{\infty} 2h_2 m G_n(0)\cos(m\pi y/2) S_{nm} \times [\sin(7\pi m/16) + \sin(5m\pi/16)] \times \{(m^2/4-16)(b_{nm})[(m\pi/2)^2 + 16\pi^2 + \lambda_n]\}^{-1}.$$

The O(1) cross channel velocity is given by $v^{(0)} = \partial_1 p^{(0)}$, i.e.,

$$v^{(0)} = \sum_{n=0}^{\infty} \partial_1 P_n G_n, \qquad \text{(A2)}$$

where $\partial_1 P_n$ is given by

$$\partial_1 P_n = h_1 G_n(0)\sin(\pi y) D_1 R_{n2} \times [2\pi(\pi^2+\lambda_n)(2\pi^2+\lambda_n)]^{-1} + \sum_{m=1}^{\infty} h_1 G_n(0) \times \sin(m\pi y/2) D_1 R_{nm}[m/2 - \sin(m\pi/4)] \times \{\pi(m^2/4-1)(b_{nm})[(m\pi/2)^2+\pi^2+\lambda_n]\}^{-1} - \sum_{m=1}^{\infty} 4h_2 G_n(0)\sin(m\pi y/2) D_1 S_{nm} \times [\sin(7\pi m/16) + \sin(5\pi m/16)] \times [\pi(m^2/4-1)(b_{nm})(16\pi^2 + b_{nm})]^{-1},$$

where the derivatives of R_{nm} and S_{nm} with respect to x are given by

$$D_1 R_{nm}(x) = -2\pi(b_{nm})^{1/2}\,\mathrm{sgn}(x)\exp[-|x|(b_{nm})^{1/2}] \times \cosh[(b_{nm})^{1/2}/2], \quad \text{if} \quad |x| > 0.5$$

$$D_1 R_{nm}(x) = -2\pi(b_{nm})^{1/2}(\sin(\pi x) - \exp[-(b_{nm})^{1/2}/2] \times \sinh[x(b_{nm})^{1/2}]), \quad \text{if} \quad |x| < 0.5$$

$$D_1 S_{nm}(x) = -8\pi(b_{nm})^{1/2}\,\mathrm{sgn}(x-0.6) \times \exp[-|x-0.6|(b_{nm})^{1/2}\cosh[(b_{nm})^{1/2}/8], \quad \text{if} \quad |x-0.6| > 0.125$$

$$D_1 S_{nm}(x) = -8\pi[(m\pi/4)^2+\lambda_n]^{1/2}(\sin[4\pi(x-0.6)] - \exp[-(b_{nm})^{1/2}/8]\sinh[(x-0.6)(b_{nm})^{1/2}]), \quad \text{if} \quad |x-0.6| < 0.125,$$

with $\mathrm{sgn}(x)$ being the sign of the variable x.

The O(1) density field is obtained from $\rho^{(0)} = -\partial_3 p^{(0)}$, i.e.,

$$\rho^{(0)} = \alpha^{-1}[1 - \exp(-\alpha y)] D_3 Z - \sum_{n=0}^{\infty} P_n D_3 G_n \qquad \text{(A3)}$$

where $D_3 G_n(z)$ and $D_3 Z(z)$ are given by

$$D_3 G_n(z) = (c_n\gamma/2)\exp(\gamma z)\{A_n J_0[c_n\exp(\gamma z/2)] + B_n Y_0[c_n\exp(\gamma z/2)]\},$$

$$D_3 Z(z) = (\lambda\gamma/2)\exp(\gamma z)\{C_1 J_0[\lambda\exp(\gamma z/2)] + C_2 Y_0[\lambda\exp(\gamma z/2)]\},$$

with the constants A_n, B_n, C_1 and C_2 as defined previously.

The O(1) vertical velocity $w^{(0)}$ is given by

$$w^{(0)} = [S(z)]^{-1} J[p^{(0)}, \rho^{(0)}], \qquad \text{(A4)}$$

obtained from the O(1) mass equation (see LeBlond and Mysak, 1978, eq. (44.36), noting that their $w^{(1)}$ is our $w^{(0)}$).

The vector valued nondimensional O(1) mass transport is defined as $\mathbf{M} = (m_1, m_2)$, with the components m_1 and m_2 given by

$$m_1 = \int_0^1 u^{(0)} dz$$

$$m_2 = \int_0^1 v^{(0)} dz.$$

These integrals can be evaluated to yield

$$m_1 = (\lambda\gamma/2)^{-1} \exp(-\alpha y) \times [C_1 J_0(x) + C_2 Y_0(x)]\Big|_{x=c_n \exp(\gamma/2)}^{x=c_n} - \sum_{n=0}^{\infty} \partial_2 P_n \times (c_n\gamma/2)^{-1}[A_n J_0(x) + B_n Y_0(x)]\Big|_{x=c_n \exp(\gamma/2)}^{x=c_n} \quad \text{(A5)}$$

$$m_2 = \sum_{n=0}^{\infty} \partial_1 P_n (c_n\gamma/2)^{-1}[A_n J_0(x) + B_n Y_0(x)]\Big|_{x=c_n \exp(\gamma/2)}^{x=c_n}. \quad \text{(A6)}$$

REFERENCES

Bennett, E. B., 1959: Some oceanographic features of the northeast Pacific Ocean during August 1955. *J. Fish. Res. Bd. Can.*, **16**, 565–633.

Bjerknes, J., 1966: A possible response of the atmospheric Hadley circulation to equatorial anomalies of ocean temperature. *Tellus*, **18**, 820–829.

Bryan, K., and P. Ripa, 1978: The vertical structure of north Pacific temperature anomalies. *J. Geophys. Res.*, **83**, 2419–2429.

Csanady, G. T., 1979: The birth and decay of a warm core ring. *J. Geophys. Res.*, **84**, 777–780.

Chao, S., L. J. Pietrafesa and G. S. Janowitz, 1980: On the dynamics of a baroclinic jet over shallow topography. Unpublished manuscript.

Emery, W. J., and K. Hamilton, 1985: Atmospheric forcing of interannual variability in the northeast Pacific Ocean, connections with El Niño. *J. Geophys. Res.*, **90**, 857–868.

——, W. G. Lee and L. Magaard, 1984: Geographic distributions of density, Brunt-Väisälä frequency and Rossby radii in the North Pacific and North Atlantic. *J. Phys. Oceanogr.*, **14**, 294–317.

Groot, C., 1982: Modifications on a theme. A perspective on migratory behaviour of Pacific salmon. *Proc. Salmon and Trout Migratory Behaviour Symp.*, E. L. Brannon and E. O. Salo, Eds., College of Fisheries, University of Washington, 1–21.

Hamilton, K., 1984: Seasonal mean North Pacific sea level pressure charts 1939–82. Department of Oceanography Manuscript Rep. No. 41, University of British Columbia, Vancouver, 177 pp.

Hogg, N. G., 1980: Effects of bottom topography on ocean currents, *Orographic Effects in Planetary Flows*. GARP Publ. Ser. No. 23., 167–265.

Horel, J. D., and J. M. Wallace, 1981: Planetary-scale atmospheric phenomena associated with the Southern Oscillation. *Mon. Wea. Rev.*, **109**, 813–829.

Huppert, H. E., 1975: Some remarks on the initiation of inertial Taylor columns. *J. Fluid Mech.*, **67**, 397–412.

Ikeda, M., L. A. Mysak and W. J. Emery, 1984: Observations and modeling of satellite-sensed meanders and eddies off Vancouver Island. *J. Phys. Oceanogr.*, **14**, 3–21.

Julian, P. R., and R. M. Chervin, 1978: A study of the Southern Oscillation and Walker circulation phenomenon. *Mon. Wea. Rev.*, **106**, 1433–1451.

Kirwan, A. D., Jr., G. S. McNally, E. Reyna and W. J. Merrell, Jr., 1978: The near-surface circulation of the eastern North Pacific. *J. Phys. Oceanogr.*, **8**, 937–945.

LeBlond, P. H., and L. A. Mysak, 1978: *Waves in the Ocean*. Elsevier, 602 pp.

Mied, R. P., and G. L. Lindemann, 1979: The propagation and evolution of cyclonic Gulf Stream rings. *J. Phys. Oceanogr.*, **9**, 1183–1206.

Mysak, L. A., W. W. Hsieh and T. R. Parsons, 1982: On the relationship between interannual baroclinic waves and fish populations in the northeast Pacific. *Bio. Oceanogr.*, **2**, 63–103.

Simpson, J. J., 1983: Large scale thermal anomalies in the California current during the 1982–1983 El Niño. *Geophys. Res. Lett.*, **10**, 937–940.

Swaters, G. E., 1983: Topographically-induced baroclinic eddies along a coastline. M.Sc. thesis, Department of Mathematics, University of British Columbia, 187 pp.

Tabata, S., 1967: Circulation of the northeast Pacific Ocean as deduced from isentropic analysis. *Int. Assoc. Phys. Sci. Ocean, Proc.-Verbaux* No. 10, 14th General Assembly, Berne, 119–120.

——, 1975: The general circulation of the Pacific Ocean and a brief account of the oceanographic structure of the North Pacific Ocean. *Atmosphere*, **13**, 133–168.

——, 1982: The anticyclonic, baroclinic eddy off Sitka, Alaska, in the northeast Pacific Ocean. *J. Phys. Oceanogr.*, **12**, 1260–1282.

Trenberth, K. E., 1976: Spatial and temporal variations of the Southern Oscillation. *Quart. J. Roy. Meteor. Soc.*, **102**, 639–653.

Willmott, A. J., and L. A. Mysak, 1980: Atmospherically forced eddies in the northeast Pacific. *J. Phys. Oceanogr.*, **10**, 1769–1791.